Geochimica et Cosmochimica Acta 384 (2024) 1–13

Contents lists available at ScienceDirect

Geochimica et Cosmochimica Acta

journal homepage: www.elsevier.com/locate/gca

Ebullition drives high methane emissions from a eutrophic coastal basin

Olga M. Żygadłowska [a,*], Jessica Venetz [b], Wytze K. Lenstra [a,b], Niels A.G.M. van Helmond [a,b], Robin Klomp [a,b], Thomas Röckmann [c], Annelies J. Veraart [d], Mike S.M. Jetten [b], Caroline P. Slomp [a,b]

[a] Department of Earth Sciences - Geochemistry, Utrecht University, Princetonlaan 8a, 3584CB Utrecht, the Netherlands
[b] Department of Microbiology, Radboud Institute for Biological and Environmental Sciences, Radboud University, Heyendaalseweg 135, 6525AJ Nijmegen, the Netherlands
[c] Institute for Marine and Atmospheric Research Utrecht, Utrecht University, Princetonplein 5, 3584CC Utrecht, the Netherlands
[d] Department of Aquatic Ecology and Environmental Biology, Radboud Institute for Biological and Environmental Sciences, Radboud University, Heyendaalseweg 135, 6525AJ Nijmegen, the Netherlands

ARTICLE INFO

Associate editor: Natascha Riedinger

Keywords:
Methane isotopes
Coastal waters
Microbial methane oxidation
Methane bubbles

ABSTRACT

The production of methane in coastal sediments and its release to the water column is intensified by anthropogenic eutrophication and bottom water hypoxia, and it is still uncertain whether methane emissions to the atmosphere will be enhanced. Here, we assess seasonal variations in methane dynamics in a eutrophic, seasonally euxinic coastal basin (Scharendijke, Lake Grevelingen). In-situ benthic chamber incubations reveal high rates of methane release from the sediment to the water column (74–163 mmol m^{-2} d^{-1}) during monthly measurements between March and October 2021. Comparison of these in-situ total benthic methane fluxes and calculated diffusive fluxes point towards a major role for ebullition. In spring and fall, when the water column was oxic, microbial removal of dissolved methane occurred aerobically in the bottom water. In summer, in contrast, dissolved methane accumulated to concentrations of up to 67 μmol L^{-1} below the oxycline. Shifts in $\delta^{13}C$–CH_4 and δD-CH_4 towards higher values and the abundant presence of methane oxidizing bacteria point towards removal of methane around the oxycline, likely through both aerobic and anaerobic pathways, with the latter possibly linked to iron oxide reduction. Shifts in $\delta^{13}C$–CH_4 and δD-CH_4 to lower values above the oxycline indicate that bubble dissolution contributed to dissolved methane. Methane emissions to the atmosphere were observed in all seasons with the highest, in-situ measured diffusive fluxes (1.2 mmol m^{-2} d^{-1}) upon the onset of water column mixing at the end of summer. Methane release events during the measurement of in-situ water-air fluxes and model calculations point towards a flux of methane to the atmosphere in the form of bubbles, which bypass the microbial methane filter. The model calculations suggest a potential year-round ebullitive methane flux between 30 and 120 mmol m^{-2} d^{-1}. We conclude that methane emissions from eutrophic coastal systems may be much higher than previously thought because of ebullition.

1. Introduction

Methane is a potent greenhouse gas (IPCC, 2023). Over the past century, the atmospheric concentration of methane has increased strongly, reaching a new record of 1921 ppb in 2023 (Lan et al., 2024). In addition to anthropogenic sources, the global methane budget is also greatly impacted by natural sources of methane, including marine environments. Coastal systems are of particular interest since they contribute up to 75 % of the total marine methane flux to the atmosphere despite accounting for only 15 % of the marine surface area (Bange et al., 1994; Rosentreter et al., 2021). Coastal environments worldwide are increasingly affected by eutrophication and deoxygenation (Breitburg et al., 2018). While such environments are frequently characterized by high methane concentrations in the water column (e.g. Reeburgh et al., 1991; Gelesh et al., 2016), it remains unclear what fraction of the methane ultimately escapes to the atmosphere (Naqvi

* Corresponding author.
E-mail addresses: o.m.zygadlowska@uu.nl (O.M. Żygadłowska), j.venetz@science.ru.nl (J. Venetz), wytze.lenstra@ru.nl (W.K. Lenstra), n.vanhelmond@uu.nl (N.A.G.M. van Helmond), robin.klomp@ru.nl (R. Klomp), t.roeckmann@uu.nl (T. Röckmann), a.veraart@science.ru.nl (A.J. Veraart), m.jetten@science.ru.nl (M.S.M. Jetten), caroline.slomp@ru.nl (C.P. Slomp).

https://doi.org/10.1016/j.gca.2024.08.028
Received 22 March 2024; Accepted 30 August 2024
Available online 1 September 2024
0016-7037/© 2024 The Authors. Published by Elsevier Ltd. This is an open access article under the CC BY license (http://creativecommons.org/licenses/by/4.0/).

et al., 2010; Weber et al., 2019; Saunois et al., 2020).

Methane is produced in anoxic sediments during organic matter degradation (Froelich et al., 1979) and can be removed through aerobic and anaerobic pathways (Boetius et al., 2000; Reeburgh, 2007; Wallenius et al., 2021). Aerobic removal refers to methane oxidation with oxygen. Anaerobic pathways include methane oxidation coupled to the reduction of sulfate (Boetius et al., 2000; Knittel and Boetius, 2009), iron and manganese oxides (Beal et al., 2009; Sivan et al., 2011; Ettwig et al., 2016), nitrate and nitrite (Ettwig et al., 2009, 2010; Haroon et al., 2013). The efficiency of methane removal in sediments is especially sensitive to the environmental setting. High rates of sediment accumulation and input of organic matter in particular can lead to such high rates of methane production that the slow-growing anaerobic methanotrophs cannot keep up (Dale et al., 2008; Egger et al., 2016; Lenstra et al., 2023). This may lead to a shoaling of the zone of methane production and enhanced release of methane to the water column (Egger et al., 2016; Lenstra et al., 2023). When the production of methane exceeds the rate of its diffusive transport, this can result in oversaturation of dissolved methane in porewaters and the formation of methane bubbles (Reeburgh, 1969; Boudreau et al., 2005). Methane in the form of bubbles can bypass the sedimentary microbial filter and directly escape into the water column (Judd et al., 1997; Leifer and Patro, 2002; Joye et al., 2004).

Dissolved methane and methane bubbles differ in their dominant pathway of vertical transport in the water column. Transport of dissolved methane is controlled by turbulent diffusion as a result of density-driven (temperature and salinity dependent) convection or wind-induced mixing (Imboden and Wüest, 1995; Read et al., 2012). When rates of turbulent diffusion are high and the water column is fully mixed, methane can be mixed upward rapidly. Such well-mixed water columns are typically also oxygenated. In stratified water columns, however, rates of turbulent diffusion will be low around the pycnocline, promoting the development of an oxycline, i.e. a transition from oxic to anoxic waters with water depth, frequently allowing accumulation of methane below the oxycline (Gelesh et al., 2016; Steinsdóttir et al., 2022). Vertical transport of methane in bubbles primarily depends on the bubble diameter and the water depth of bubble release, with smaller bubbles and deeper waters promoting dissolution of methane in the water column (McGinnis et al., 2006). Bubble dissolution is critical for methane removal since methane bubbles are not subject to microbial oxidation.

Removal of dissolved methane primarily involves methane-oxidizing bacteria (MOB), and archaea. In a water column where an oxycline is present, most methane is expected to be removed aerobically in the zone where methane directly meets oxygen (Schmale et al., 2010; Steinle et al., 2017; Venetz et al., 2023). Recent work has shown that the MOB that are typically responsible for aerobic methane removal can also be active in anoxic waters and utilize electron acceptors other than oxygen. Such removal of methane below the oxycline has been linked to aerobic methanotrophic bacteria of the *Methylococcales* family, with the methane oxidation being coupled to partial denitrification (Padilla et al., 2017; Steinsdóttir et al., 2022). In a recent study for freshwater sediments, these aerobic methanotrophs were also found to couple methane oxidation to iron(III) reduction (Li et al., 2023), but whether this holds for coastal waters is not known. Potential anaerobic methanotrophs include "Candidatus *Methanoperedens*" of the archaeal ANME-2d cluster, which are known to link methane oxidation to nitrate, iron(III) and manganese(IV) reduction (Ettwig et al., 2010, 2016; Leu et al., 2020) and Ca. *Methylomirabilis*, which produces the oxygen needed for methane oxidation through dismutation of nitric oxide from nitrite reduction (Ettwig et al., 2010; Padilla et al., 2016; Thamdrup et al., 2019). Microbial methane oxidation leads to a distinct change in the isotopic composition of methane (Whiticar and Faber, 1986). As microbes preferentially remove lighter C and H isotopes (i.e. prefer ^{12}C over ^{13}C and H over D), methane oxidation leads to enrichment of the residual methane in the heavier isotopes. This is reflected in a positive shift in both $\delta^{13}C\text{-}CH_4$ (Whiticar, 1999) and $\delta D\text{-}CH_4$ (Coleman et al., 1981). Stable methane isotopes therefore provide a tool to track microbial methane oxidation in marine environments (Whiticar, 1999).

Progressive eutrophication of coastal systems is expected to enhance the methane flux from sediments (Crill and Martens, 1987; Gelesh et al., 2016; Lenstra et al., 2023). Eutrophication not only enhances the rate of methane production in the sediment, but also reduces the rate of bubble dissolution in the water column because larger bubbles are formed (McGinnis et al., 2006) that are more resistant to dissolution (Delwiche and Hemond, 2017). Hence, the chance of methane bubbles reaching the atmosphere is particularly high in eutrophic systems (Boudreau et al., 2005) with a water depth that is less than 100 m (McGinnis et al., 2006; Ostrovsky et al., 2008). Despite the large potential for bubble-associated methane release from coastal waters (Rosentreter et al., 2021), we still know little about the contribution of bubbles to methane emissions from these systems.

Building on results from a previously published dataset that used samples collected during 2020 (Żygadłowska et al., 2023), here we investigate water column methane dynamics in a eutrophic coastal system (Lake Grevelingen, Netherlands) between March and October 2021. We assess the seasonal changes in dissolved methane and its isotopes ($\delta^{13}C\text{–}CH_4$ and $\delta D\text{-}CH_4$) and methane oxidizing bacteria and archaea in the water column. Using incubations with an in-situ benthic flux chamber (sum of diffusive and ebullitive flux), a floating chamber at the water–air interface (diffusive flux and ebullitive flux events) and calculations (diffusive and ebullitive flux), we also assess the seasonality in methane emissions across the sediment–water and water–air interface.

2. Materials and methods

2.1. Study area

Marine Lake Grevelingen is a former estuary of the river Rhine that was dammed at the landward side in 1964 and at the North Sea side in 1971. While the average depth of the lake is ~5 m, it is intersected by deeper former tidal channels, which connect several basins that range in depth from 34 to 45 m (Hagens et al., 2015; Egger et al., 2016). Sluices in the dam at the seaward side enable daily water exchange with the North Sea since 1999. This sets the lake salinity to relatively constant values of 29–33. The water exchange generally has little effect on the vertical mixing of the water column in the lake, but occasional lateral inflows into the deep basins are possible (Hagens et al., 2015; Sulu-Gambari et al., 2017). The lake receives large amounts of algal material from the adjacent North Sea in summer. This contributes to its highly eutrophic state (Hagens et al., 2015).

In this study, we focus on the deepest basin in the lake (Scharendijke basin; 51.742°N, 3.849°E; Figure S1), which has a water depth of 45 m (Egger et al., 2016). The water column in the basin is seasonally stratified between May and September and the bottom waters are typically euxinic in summer (Egger et al., 2016; Żygadłowska et al., 2023). The sediments are fine-grained and receive a high input of organic matter (~250 mmol C m^{-2} d^{-1}; Egger et al., 2016), which contributes to high rates of methane production (Egger et al., 2016; Żygadłowska et al., 2023). The water column in Scharendijke basin shares many general characteristics (e.g. seasonal variation in density stratification and redox gradients) with those of fjords (e.g. Jorgensen, 1980; Steinsdóttir et al., 2022), coastal bays (e.g. Turner et al., 1987; Ma et al., 2020) and large estuaries (e.g. Kemp et al., 1992; Gelesh et al., 2016).

Sampling of the water column and sediment as well as in-situ benthic and floating chamber deployments were performed during 9 sampling campaigns with the RV *Navicula* between March and October 2021. Depth profiles of dissolved oxygen, temperature and salinity were obtained using a CTD (Seabird SBE 911 plus) equipped with an oxygen sensor (Seabird SBE43). Oxygen sensors are commonly not accurate enough to record the absence of oxygen in marine waters (Grégoire

et al., 2021). Here, we consider waters to be anoxic when concentrations are close to zero and the profile becomes a vertical line. For salinity, we use the practical salinity scale.

2.2. Water column sampling

Discrete water samples were collected using a 10 L Niskin bottle at a depth resolution of 1–2 m during each sampling campaign. Samples were collected for the analysis of methane and its isotopic composition (δ^{13}C-CH_4 and δD-CH_4), sulfide, ammonium, nitrate, nitrite and total and dissolved manganese and iron. For methane analyses, serum bottles of 120 mL were filled from the bottom up with water directly taken from the Niskin bottle and were allowed to overflow. The bottles were closed with butyl rubber stoppers and crimped with aluminum caps ensuring that no air bubbles remained inside. All samples were poisoned with a 0.25 mL saturated mercury chloride solution directly after collection, and stored upside down in the dark.

For sulfide, 0.5 mL of sample was filtered through a 0.2 μm nylon syringe filter directly into a glass vial pre-filled with 2 mL of a 2 % zinc acetate solution and stored at 4 °C. Water column samples for ammonium, nitrite and nitrate were filtered through 0.2 μm nylon syringe filters and stored at −20 °C. Samples for total dissolvable (henceforth termed "total") and dissolved iron and manganese were collected directly from the Niskin bottle using acid-washed 250 mL LDPE Nalgene bottles and Tygon 5000 tubing. The acid-washing (see Supplementary Material, Section S1.1) was performed to avoid trace metal contamination (Cutter et al., 2017). For dissolved iron and manganese, the samples were filtered directly from the Niskin bottle using a 0.2 μm Sartobran 300 cartridge filter. Both unfiltered and filtered samples were then acidified with concentrated ultrapure HCl (200 μL of acid per 100 mL of sample). Samples for total iron and manganese were filtered with a 0.45 μm nylon filter exactly 6 months after collection, to ensure that the exposure time of the particles to acid was identical for each set of unfiltered samples. The sample handling and chemical analysis for sulfate is described in the Supplementary Material (section S1.2).

2.3. Sediment and porewater sampling

During each sampling campaign, three sediment cores were collected using a UWITEC corer and PVC core liners (120 cm length, 6 cm inner diameter). Methane samples were collected immediately from one core after retrieval using a liner with two lines of holes drilled at 5 cm intervals on opposite sides of the liner offset by 2.5 cm and covered with tape. From each hole, 10 mL of sediment was taken with a cut-off plastic syringe and transferred into a 65 mL glass bottle filled with saturated NaCl solution. The bottles were topped up with NaCl, closed with rubber stoppers and aluminum screw caps and stored upside down until analysis. Note that methane degassing may occur during sample collection (Kiene and Capone, 1985), leading to an underestimation of methane concentrations (Egger et al., 2017; Jørgensen et al., 2019). This effect intensifies with higher concentrations of methane, but does not significantly impact its isotopic composition (Wallace et al., 2000; Egger et al., 2017). A second sediment core was sliced for the sediment porosity which is determined based on the weight loss of each sediment sample upon oven-drying, assuming a sediment density of 2.65 g cm^{-3} (Burdige, 2006). A third sediment core was sliced to determine porewater profiles of sulfate, sulfide and alkalinity for each sampling campaign and sediment organic carbon contents for four months (upper 30 cm), namely March, June, August and September (Supplementary section S1.3).

2.4. Chemical analysis

To determine methane concentrations in the water column samples, 10 mL of nitrogen gas was added to each sample while simultaneously removing the same volume of liquid. Methane concentrations were measured with a Thermo Finnigan Trace™ gas chromatograph (Flame Ionization Detector; limit of detection 0.02 μmol L^{-1}) following gas and water phase equilibration (>2h for water column samples and 7 days for sediment samples). The analysis of stable methane isotopes (δ^{13}C-CH_4 and δD-CH_4) was conducted using Continuous Flow Isotope Ratio Mass Spectrometry (CF-IRMS) as described by Brass and Röckmann (2010) and Sapart et al., (2011).

Sulfide concentrations were determined using the phenylenediamine and ferric chloride method (Cline, 1969). The indophenol blue method (Solorzano, 1969) was used to measure ammonium. Nitrite and nitrate concentrations were determined with a Gallery™ Automated Chemistry Analyzer type 861 (Thermo Fisher Scientific). The total and dissolved concentrations of iron and manganese were determined by inductively coupled plasma mass spectrometry (ICP-MS, Perkin Elmer NexION 2000). The samples were concentrated in order to remove the seawater matrix using a SC-DX SeaFAST S2 (Elemental Scientific) prior to analysis (Lenstra et al., 2022). Further details are given in the Supplementary Material (section S1.4). Where the dissolved fraction of iron is slightly higher than the total fraction (here observed in samples from below a water depth of 35 m), this is attributed to an analytical artifact linked to high sulfide concentrations as observed previously (Lenstra et al., 2021).

2.5. Methanotrophs in the water column

To obtain insight in the vertical distribution of methanotrophs in the water column, 1 L of seawater was collected from selected depths in March, July, August, end of August and October for DNA analysis and filtered through 0.22 μm PES Supor filters using a vacuum pump. The filters were stored at −80 °C directly after collection. The DNA collected on the filters was extracted using a FastDNA™ SPIN Kit for Soil DNA isolation (MP Biomedicals). The microbial community composition was analyzed by sequencing the V3-V4 region of the 16S rRNA gene (Ilumina MiSeq platform, Macrogen) as described in Venetz et al., (2024). 16S rRNA sequencing data for bacteria were obtained for five months, while those for archaea were obtained for July, August, end of August and September.

2.6. In-situ total benthic methane flux

In-situ total benthic fluxes of methane (sum of diffusive and ebullitive flux) were measured using a MiniChamber Lander System (Unisense) equipped with a metal-free polycarbonate incubation chamber (30 × 30 × 35 cm), with a lid at the top, and a set of twelve 50 mL plastic syringes controlled by an autosampler and connected to the chamber with plastic tubing. The adjustable feet of the lander enabled the incubation chamber to sink 7 cm into the sediment, leaving a water volume in the chamber of 25.2 L, which, together with its surface area of 0.09 m^2, was used to calculate the in-situ benthic fluxes of methane. Lander deployments were conducted after all water column and porewater sampling was completed. The lander was lowered onto the sediment at a low speed with an open lid. The sampling sequence started after a 40 min delay period to allow potential resuspended sediment to settle before sampling started. A stirrer attached to the lid gently mixed the water in the chamber. The stirring is expected to have led to dissolution of methane bubbles that were released from the sediment. Each deployment consisted of 5 timepoints (25–30 min apart from each other). For each timepoint, two syringes were filled to ensure enough water was collected to allow the sample vials for methane to overflow. A small septum in the lid of the chamber ensured replacement of the water that was withdrawn. Upon retrieval each sample was transferred to a 65 mL serum bottle, closed with a rubber stopper and an aluminum screw cap, poisoned with 0.1 mL of saturated mercury chloride solution and stored upside down in the dark until analysis. Methane concentrations were determined as described in section 2.4. In-situ total benthic fluxes of methane in mmol m^{-2} d^{-1} were calculated from the change in concentration of methane in the chamber with time, using linear regression and accounting for the volume of the chamber and its area.

2.7. Benthic diffusive methane flux (calculated)

Diffusive fluxes of methane across the sediment–water interface were calculated according to Fick's first law based on the concentration gradient in methane between the first porewater sample and the bottom water:

$$J = -\phi Ds\frac{dC}{dz} \quad (1)$$

where J is the diffusive flux in mmol m^{-2} d^{-1}, ϕ is the porosity of the sediment, Ds is the diffusion coefficient for methane in the sediment in m^{-2} d^{-1}, C is the concentration of methane in mmol m^{-3} and z is the sediment depth in m. Ds is calculated from the diffusion coefficient for methane in seawater, corrected for salinity and temperature using the R package CRAN: marelac (Soetaert et al., 2010), accounting for the tortuosity of the sediment (Boudreau, 1996). Methane concentrations were determined as described in section 2.4.

2.8. In-situ water–air methane flux (diffusive flux and ebullitive flux events)

In-situ water–air methane fluxes were measured with a floating chamber (Venetz et al., 2024) on the same day as the water column sampling. The transparent acrylic cylindric floating chamber (390 mm diameter), was connected to a LICOR trace gas analyzer (LI-7810) forming a closed loop. Fluxes were measured in triplicate, with each measurement lasting 3–10 min, until a linear change was observed. The chamber was ventilated after each measurement until atmospheric methane concentrations were reached. Water-air fluxes were calculated as described in the Supplementary Material (section S1.5).

Instances of sudden increases in methane concentrations due to bubbles entering the chamber occurred 1 to 12 times per sampling campaign during 5 cruises. Those data were removed from the diffusive flux calculations and, in cases where the ebullitive flux was monitored, were used to estimate the order of magnitude of the bubble flux instead. The bubble flux was estimated based on the change of the methane concentration in the chamber and the number of bubble events per sampling campaign (Supplementary Material S1.6; Figure S2.). Due to high winds, deployments of the benthic and floating chambers were not possible in May.

2.9. Water-air diffusive methane flux (calculated)

Diffusive fluxes of methane across the water–air interface were determined as follows:

$$F_{atm} = kK_o(C_W - C_O) \quad (2)$$

where F_{atm} represents the diffusive flux from the water column to the atmosphere in mmol m^{-2} d^{-1}, k is the gas exchange coefficient in m d^{-1}, K_o is the aqueous-phase solubility of methane and C_W and C_O are the measured concentrations of methane in the water at 1 m depth and in the air, respectively (Humborg et al., 2019). Further details are given in the Supplementary Material section S1.7.

2.10. Water-air ebullitive methane flux (model-calculated potential range)

The potential range of the ebullitive methane flux to the atmosphere was estimated from model results described by McGinnis et al., (2006) using the water depth of Scharendijke basin (45 m), the benthic bubble flux of methane (i.e. the rate of release of methane bubbles at the sediment–water interface), and an assumed diameter of the methane bubbles as input parameters. The model provides an estimate of the percentage of the methane that dissolves in the water column (with the remainder then being emitted to the atmosphere). The bubble flux of methane from the sediment to the water column in Scharendijke basin was calculated as the difference between the in-situ total benthic methane flux and the calculated diffusive flux. To estimate an average and maximum bubble flux, we assumed a bubble diameter of 10 and 20 mm, respectively, in accordance with the average and maximum bubble diameter given by McGinnis et al., (2006). Based on the model, the estimated bubble emission to the atmosphere at our site could range on average from 0 to 40 % of the initial bubble flux at the sediment–water interface meaning that 60–100 % of the bubbles dissolve in the water column before they reach the atmosphere. For the estimated maximum flux, the bubble emission to the atmosphere would range from 0 to 75 % of the initial benthic bubble flux, with 25–100 % of the bubbles dissolving in the water column.

2.11. Methane bubble dissolution in water above the oxycline

To calculate the contribution of bubble dissolution to total methane concentrations in the upper part of the water column, we applied a simple isotopic mass balance:

$$C_s Iso_s = C_{diff} Iso_{diff} + C_{bubb} Iso_{bubb} \quad (3)$$

where C_s is the concentration and Iso_s is the isotopic signature ($\delta^{13}C$) of methane in the water above the oxycline where methane is most depleted in ^{13}C, i.e. the depth with the maximum impact of bubble dissolution. Iso_{diff} represents the isotopic signature of the methane that has diffused upwards and is approximated by the signature at the depth near the oxycline with the strongest enrichment in ^{13}C. Iso_{bubb} represents the isotopic signature of the methane supplied through bubbles, which is approximated by the signature determined closest to the sediment–water interface. C_{diff} and C_{bubb}, in turn, represent the concentration of methane in the surface water supplied through diffusion and bubble dissolution, respectively.

3. Results

3.1. Water column salinity, temperature and oxygen

The salinity in Scharendijke basin increased slightly with water depth from values around 29 in the surface waters to ca. 31 at depth and showed little change throughout the year (Fig. 1). This contrasted strongly with the large seasonal changes in temperature and oxygen. While in March and April the water column still had a constant temperature of around 8 °C and was oxygenated, temperature-induced density stratification led to the formation of three distinct layers in the water column from May onwards, with a warm, oxic surface layer (0–15 m) overlying a colder middle layer with variable oxygen content (15–35 m) and an even colder anoxic bottom layer (35–45 m). In August and September, the temperature throughout the water column gradually increased, indicating the beginning of mixing. In October, the water column was fully mixed again as evident from the uniform temperatures of around 15 °C and the abundant presence of oxygen at all water depths. Sulfate concentrations in the water column followed salinity and increased slightly below the surface waters to values of ~25 mmol L^{-1} in all months (Figure S3).

3.2. Water column depth profiles

The water column chemistry in the basin showed relatively little change from March to May (Fig. 2; Figure S4). Oxygen was present throughout the water column and hydrogen sulfide and methane concentrations remained low at all water depths. The subsequent stratification of the water column contributed to the development of anoxia from June onwards and allowed for the accumulation of hydrogen sulfide in the bottom layer, i.e. below 36 m (Fig. 2). While in June the oxycline was present at a depth of 36 m (Table 1), the anoxia expanded

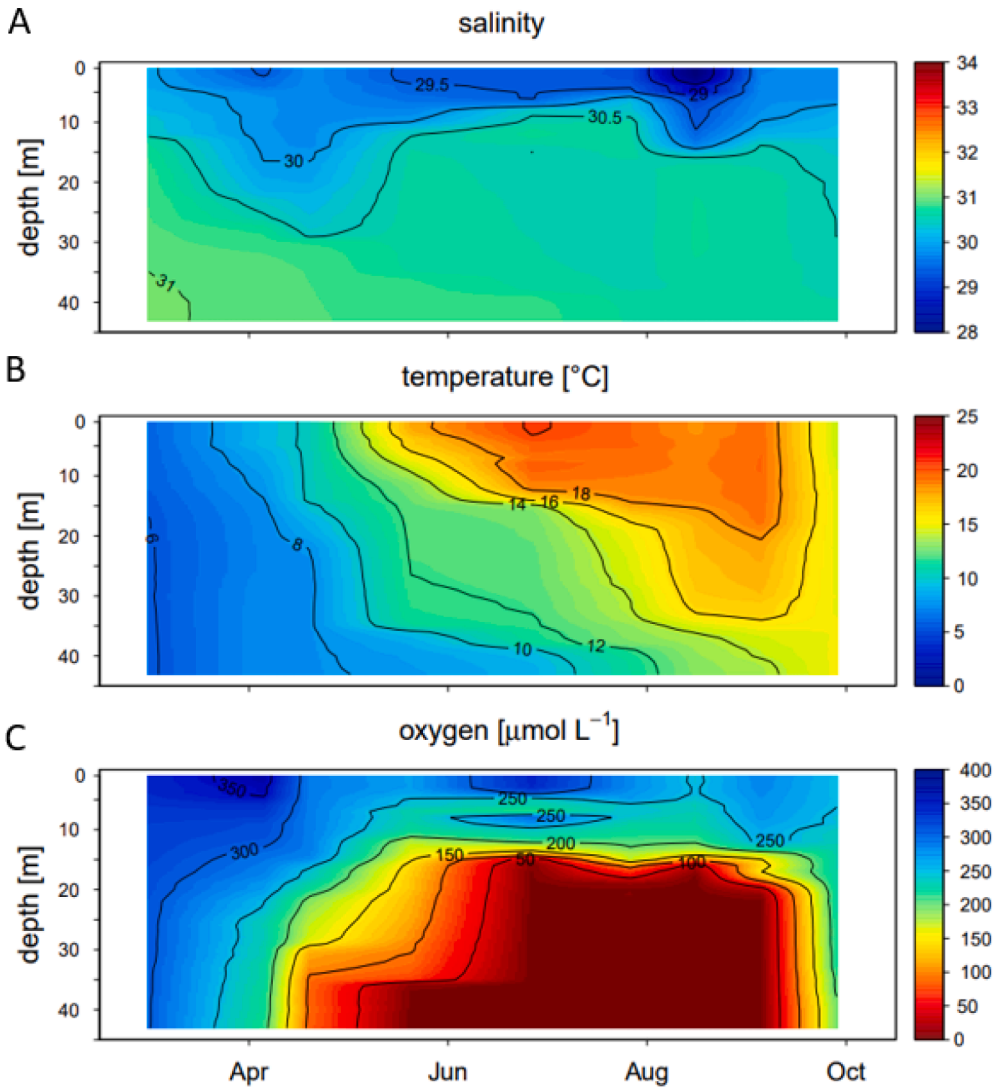

Fig. 1. Seasonal dynamics of A) salinity, B) temperature and C) oxygen in the water column between March and October 2021 in Scharendijke basin (Lake Grevelingen).

upwards to a depth of around 15 m in July, leading to the development of a suboxic, i.e. anoxic and non-sulfidic zone. Hydrogen sulfide was continuously present in the bottom water layer of the water column from June to September, at variable concentrations, ranging from 54 to 141 µmol L^{-1}, until full mixing of the water column in October.

Concentrations of ammonium, nitrate and nitrite in the water column showed a distinct seasonality. While ammonium was near zero in March, it accumulated in the lower and middle part of the water column from April to August, when a maximum concentration of 400 µmol L^{-1} was reached (Fig. 2; Figure S4). From the end of August onwards, ammonium concentrations gradually decreased again, especially in the middle part of the water column. Mixing of the water column in October led to a return to ammonium concentrations close to zero at all water depths. Nitrate concentrations, in contrast, were highest from March to May and in October, and, with the exception of the waters near the oxycline in August and September when a maximum was observed near the oxycline, were mostly very low in summer. Nitrite also showed a pronounced maximum near the oxycline in August and September, with concentrations up to 20 µmol L^{-1}. At other times of the year, nitrite was largely absent.

Dissolved iron concentrations were low from March to May and in October. From June onwards, however, substantial dissolved iron was present in the waters below the oxycline, especially in the bottom layer below 35 m depth. Total iron, which is a measure of both dissolved and particulate iron, showed an even more distinct seasonality, with elevated concentrations in the oxic water column between March and May and in October, indicating a relatively high abundance of particulate iron in the water column at this time. In July and August, particulate iron was also present above and/or below the oxycline. For the total and dissolved manganese profiles, we refer to the Supplementary Material (Section S2.1, Figure S4.).

Water column methane concentrations were below 1.4 µmol L^{-1} between March and May but methane accumulated below the oxycline from June to September, with a maximum bottom water value of 67 µmol L^{-1} (Fig. 2; Table 1). Methane concentrations in the surface water varied throughout the year from 0.04 to 0.40 µmol L^{-1}, with the highest values observed in April, end of August and in September (0.24, 0.25 and 0.40 µmol L^{-1}, respectively; Table 1). Methane concentrations in the upper 15 m of the water column showed variable trends with depth (Figure S5).

The methanotrophic community in the water column was dominated by MOB within the family of the *Methylomonadaceae* (for further details see Venetz et al., 2024). In March, less than 0.4 % of all 16S rRNA gene reads were affiliated to MOB in the water column. The abundance of the MOB increased upon stratification and the development of anoxia in the middle and lower part of the water column (Fig. 2). The MOB were

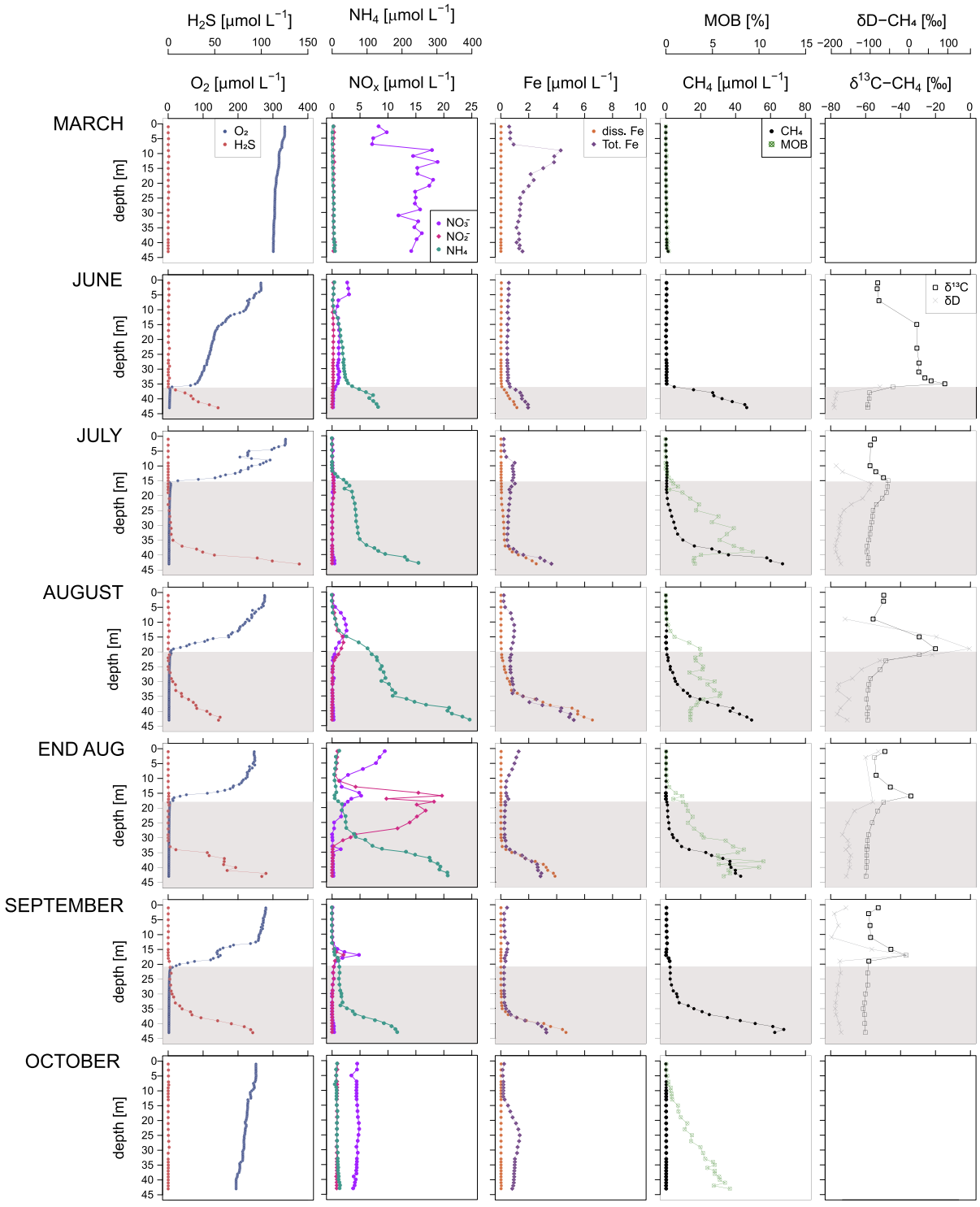

Fig. 2. Water column depth profiles of oxygen, sulfide, ammonium, nitrate and nitrite total (Td) and dissolved (d) iron, methane, methane oxidizing bacteria (MOB) and methane isotopes ($\delta^{13}C$ given in ‰ vs. VPDB (Vienna Pee Dee Belemnite); δD given in ‰ vs. V-SMOW (Vienna Standard Mean Ocean Water)) of each sampling event in March and between June and October 2021. Profiles for April and May are shown in Supplementary Material (Figure S4). Shaded areas represent anoxic parts of the water column.

mostly found near and below the oxycline. In October, the abundance of MOB increased with depth, with the highest relative abundance observed near the sediment–water interface. The relative abundance of MOB in the upper 10 m of the water column was low in all five months that were sampled for 16S rRNA analysis.

The total abundance of archaea in the water column was a factor 50–100 lower than the abundance of bacteria (Venetz et al., 2024). Methanotrophic archaea, here mainly *Methanoperedenaceae*, accounted for 2 % or less of all archaeal 16 s rRNA reads and their relative abundance did not show any coherent pattern with water depth (Table S1). ANME-2ab were only present in low abundance at a few depths (Table S1).

A strong increase in $\delta^{13}C$ – CH_4 and in δD – CH_4 values with decreasing water depth was seen near the oxycline from June to

Table 1
Date of sample collection, water depth at which oxygen was depleted (oxycline depth) and surface (1 m) and bottom (43 m) water concentrations of methane for water samples collected with the Niskin bottle. N.a.: not applicable.

Sampling month	Sampling date	Oxycline depth [m]	CH_4 [μmol L^{-1}]	
			Surface waters	Bottom waters
March	17-03-21	none	0.04	1.37
April	21-04-21	none	0.24	0.15
May	04-05-21	none	0.11	0.80
June	05-06-21	36	0.16	17.38
July	12-07-21	15	0.10	66.87
August	11-08-21	20	0.06	49.17
End Aug	31-08-21	18	0.25	42.90
September	20-09-21	22	0.40	62.41
October	13-10-21	none	0.10	0.24

September, with the highest values observed in June ($\delta^{13}C$ – CH_4: −15 ‰) and in August (δD – CH_4: 127 ‰) (Fig. 2). While the isotopic enrichment for methane was restricted to waters above the oxycline in June and September, this did not hold for July and August; in the profiles for these months, most of the increase with decreasing water depth was observed below the oxycline.

The methane isotopic signatures of the surface water differed from those around the oxycline and were largely similar to those in the bottom water. The isotopic mass balance shows that between 37 and 94 % of the methane in waters above the oxycline is supplied through bubble dissolution (Table 2).

3.3. Total and diffusive release of methane from the sediments

The in-situ total benthic fluxes of methane measured with the lander were high during all sampling campaigns, ranging from 73.9 mmol m^{-2} d^{-1} (April) to 162.9 mmol m^{-2} d^{-1} (March; Fig. 3; Table 3). Porewater concentrations of methane in the sediment were high during all months, reaching maximum values of up to 6.8 mmol L^{-1} (Figure S6). Further details on the sediment porewater chemistry and organic carbon contents are provided in Supplement S2.2. Calculated diffusive fluxes of methane from the sediment to the bottom water ranged from 0.7 to 3.8 mmol m^{-2} d^{-1} (Table 3) and hence can account for only a minor fraction of the in-situ measured benthic fluxes. Although there was quite some variability from month to month in the calculated diffusive flux, there was no distinct trend with time.

3.4. In-situ and calculated fluxes of methane to the atmosphere

The in-situ diffusive flux of methane from the water column to the atmosphere measured with the floating chamber ranged from 0.01 to 1.15 mmol m^{-2} d^{-1} and was highly variable throughout the year (Table 3, Fig. 4). The highest flux was observed in April and at the end of August and in September, while the lowest fluxes were measured in March and June. The calculated diffusive flux of methane to the atmosphere was of the same order of magnitude as the in-situ measured flux and showed a similar trend with time.

The model-estimated average and maximum bubble flux to the atmosphere, following McGinnis et al., (2006), ranged from 30 to 64 and 55 to 120 mmol m^{-2} d^{-1}, respectively (Table 3). The events of bubbles entering the floating chamber during measurements were highly variable and irregular throughout the year. The bubble flux based on events for which the methane release was monitored ranged from 0.5 to 245.3 mmol m^{-2} d^{-1} (Table 4).

Table 2
Estimation of the contribution of bubble dissolution to methane concentrations in the waters above the oxycline where methane was most depleted in ^{13}C, i.e. the depth with the maximum impact of bubble dissolution, based on the methane isotope data and mass balance.

Sampling month	Water depth [m]	Methane concentration above oxycline	Contribution from diffusion	Contribution from bubble dissolution	
		(μmol L^{-1})	(μmol L^{-1})	(μmol L^{-1})	(%)
June	23	0.11	0.07	0.04	37
July	10	0.74	0.07	0.67	91
August	9	0.44	0.03	0.41	94
End Aug	9	0.13	0.03	0.10	78
September	11	0.58	0.07	0.51	87

4. Discussion

4.1. Benthic release of methane in the form of bubbles

In-situ rates of total benthic methane release in Scharendijke basin are high throughout the year (range of 74–163 mmol m^{-2} d^{-1}; Table 3). Importantly, the average diffusive flux of methane across the sediment–water interface, was only 2 mmol m^{-2} d^{-1}. Diffusive flux calculations should be regarded as approximations (e.g. D'Ambrosio and Harrison, 2022), but an underestimation of the diffusive methane gradient of two orders of magnitude is unlikely. Hence, this suggests that diffusion was responsible for only a minor fraction of the total methane release from the sediments, which implies that a large proportion of the methane must be escaping into the water column in the form of bubbles.

The benthic methane fluxes observed here are high when compared to those at many other coastal sites (Wallenius et al., 2021; Rosentreter et al., 2021). However, the benthic methane fluxes are not unreasonably high as the input of organic matter to the sediments at this site is at least a factor two higher: reactive transport modeling of porewater ammonium profiles points towards an organic matter input of ~ 250 mmol C m^{-2} d^{-1} (Egger et al., 2016). Furthermore, the similarity in methane concentrations measured near the sediment–water interface in samples collected with three different techniques (benthic lander, water column sampling, porewater sampling; Table S2) shows that strong effects of enhanced gas release from the sediments due to disturbance of the sea floor with the benthic lander are highly unlikely. Nonetheless, to our knowledge, these in-situ benthic fluxes (74–163 mmol m^{-2} d^{-1}) are higher than those observed so far in other similar eutrophic coastal systems. For example, benthic methane fluxes of up to 9 mmol m^{-2} d^{-1} and up to 35 mmol m^{-2} d^{-1} were observed for the organic-rich sediments in the coastal basin of Cape Lookout Bight (Klump and Martens, 1980) and in eutrophic Puck Bay (Reindl and Bolałek, 2014), respectively. Our observed methane fluxes are closer to rates observed in freshwater lakes (Rosentreter et al., 2021). For example, in shallow eutrophic Lake Wohlen, a total benthic ebullition flux of 51 mmol m^{-2} d^{-1} was observed (DelSontro et al., 2015). Our work illustrates that eutrophication may allow for much higher benthic fluxes of methane from sediments in coastal bays and fjords than commonly considered. Importantly, Scharendijke basin has a marine salinity of ~ 30, implying that the abundant presence of sulfate as an electron acceptor does not safeguard such coastal systems against high rates of benthic methane release.

Organic matter input into Scharendijke basin differs seasonally, with higher inputs in summer. Bottom water redox conditions also vary seasonally, with bottom water euxinia establishing in summer (Fig. 2; Egger et al., 2016; Żygadłowska et al., 2023). The in-situ benthic flux of methane (Table 3) does not follow such a seasonal pattern, however, in line with previous work for this site showing only minor seasonal changes in sediment methane dynamics (Egger et al., 2016; Żygadłowska et al., 2023). Instead, we suggest that the benthic flux driven by bubbles is variable due to the stochastic nature of bubble release (Bastviken et al., 2004; Wik et al., 2013). Notably, our results contrast with those of a recent study of fjord sediments in which

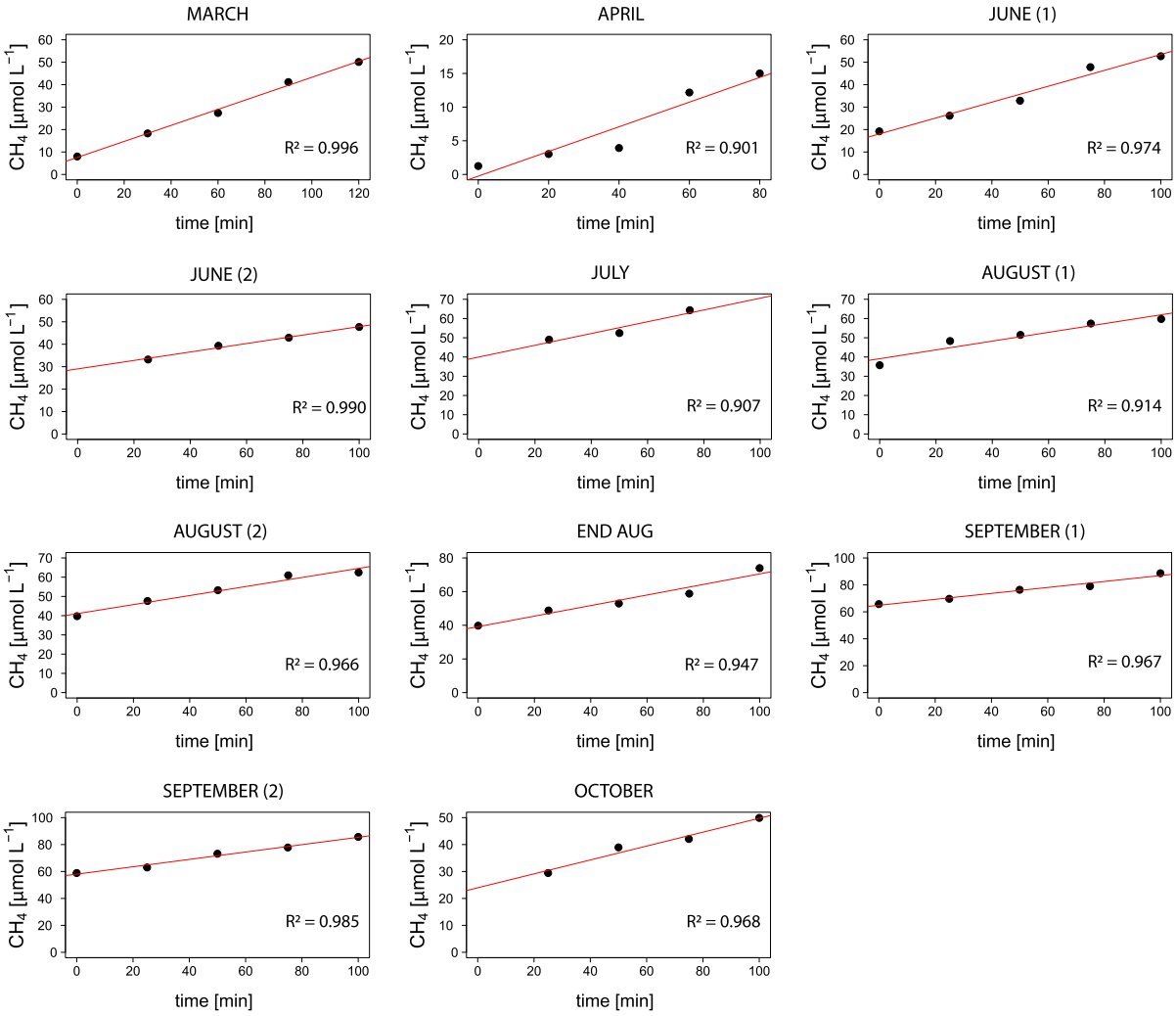

Fig. 3. Methane concentrations in the benthic lander chamber versus time. Fluxes were calculated using linear regression. The values of R^2 were always above 0.9.

Table 3
Total in-situ and calculated diffusive flux of methane at the sediment-water interface, in-situ diffusive flux and calculated diffusive flux of methane at the water-air interface and model-estimated flux of methane bubbles to the atmosphere. All fluxes are given in mmol m^{-2} d^{-1}. n.a.: not available.

Sampling month	In-situ total benthic flux of methane (diffusive + ebullitive)	Diffusive flux of methane at the sediment-water interface	In-situ flux of methane at the water-air interface (diffusive)	Calculated average diffusive methane flux at the water-air interface	Potential range of ebullitive methane flux to the atmosphere based on the model by McGinnis et al. (2006) - see section 2.10	
					Average (10 mm bubble diameter)	Maximum (20 mm bubble diameter)
March	162.9	2.9	0.01 ± 0.01	0.05	64	120
April	73.9	1.1	0.66 ± 0.29	0.55	30	55
May	n.a.	3.8	n.a.	0.37	n.a.	n.a.
June	109.4 ± 33.5	1.8	0.12 ± 0.06	0.21	43	81
July	123.4	2.1	0.22 ± 0.06	0.14	49	91
August	93.5 ± 1.4	2.0	0.17 ± 0.16	0.04	37	69
End Aug	126.4	0.7	0.96 ± 0.14	0.96	50	94
September	99.7 ± 10.7	1.1	1.15 ± 0.19	0.56	39	74
October	104.0	3.7	0.38 ± 0.18	0.20	40	75

reoxygenation of surface sediments led to a lower benthic methane fluxes (Bonaglia et al., 2022). This may be due to a lower contribution of ebullition in the fjord sediments. At Scharendijke, most methane escapes in the form of bubbles and therefore can bypass the benthic microbial filter, regardless of the bottom water redox state (Egger et al., 2016; Żygadłowska et al., 2023). To allow for such a high bubble flux persistently throughout the year, methane production must exceed methane oxidation and methane must be oversaturated in the pore waters, which is the case at this site (Egger et al., 2016; Żygadłowska et al., 2023). This highlights the role of eutrophication as a key driver of methane release to the water column: above a certain site-dependent threshold, all additional methane produced may bypass the zone of methanotrophic oxidation and will be released to the water column in the form of bubbles.

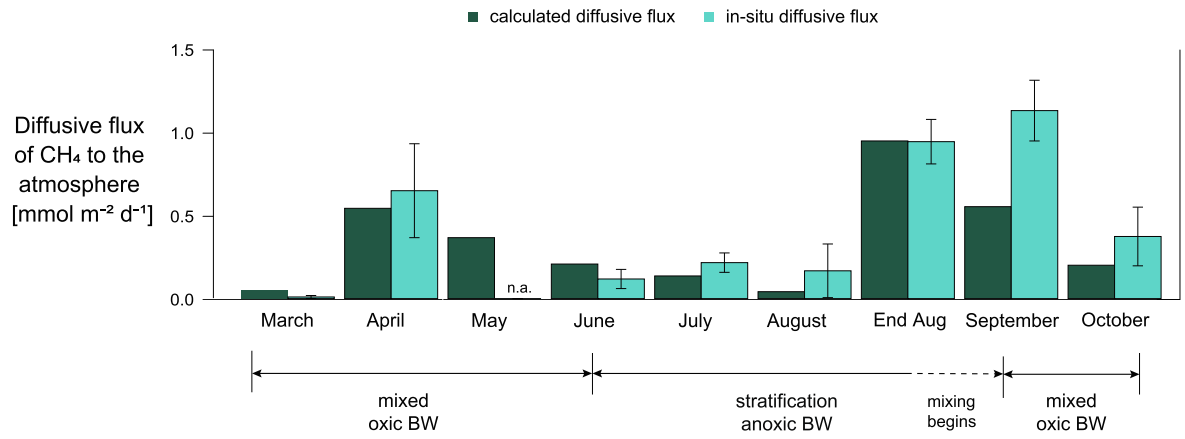

Fig. 4. Calculated and in-situ measured diffusive fluxes of methane to the atmosphere (in mmol m^{-2} d^{-1}). In-situ water–air fluxes of methane were measured with floating chambers (in triplicate).

Table 4
Bubble fluxes estimated based on events when bubbles entered the floating chamber during measurements. The bubbles were caught in the chamber on 5 separate occasions throughout the year.

Sampling month	Bubble flux [mmol m^{-2} d^{-1}]
April	63.6
June	8.7
End Aug	18.7
September	245.3
October	0.5

4.2. Seasonality in methane removal pathways

The dynamics of dissolved methane in the water column of Scharendijke basin were strongly affected by temperature-driven stratification during the summer months. Stratification of the water column not only limited the downward supply of oxygen but also allowed hydrogen sulfide, methane and ammonium to accumulate in the middle and deeper water (Figs. 2 and S7; Supplement S2.3). Even though the stratification persisted throughout the summer, the trends in hydrogen sulfide and methane in the bottom layer between July and August (Figs. 2 and S6) suggest removal of these reduced compounds. We hypothesize that either vertical or lateral flow may have contributed to this removal, starting in July. A role for vertical flow is supported by the gradual weakening of water column stratification because of warming of the water column in the summer months (Fig. 1), allowing for an enhanced downward supply of oxygen and upward transport of reduced substances in the summer months, prior to the full mixing that occurred in October.

In March and October, when the water column was fully oxic, the relative abundance of the MOB was highest in the bottom water and in the lower part of the water column, respectively (Fig. 2; Venetz et al., 2024). This points towards aerobic removal of methane. Nevertheless, relatively high methane concentrations (0.04–0.24 μmol L^{-1}), were still found in the surface waters in spring (Table 1). This is likely the result of a combination of bubble dissolution and upward mixing of methane in the well-mixed water column where turbulent transport of methane can be faster than its removal by aerobic bacteria (Gelesh et al., 2016; Borges et al., 2016). We consider a role for aerobic methane production in surface waters (e.g. Perez-Coronel and Benan, 2022) unlikely because, in coastal systems, rates of such production are low relative to rates of methane release from sediments (Kanwischer et al., 2023; Resplandy et al., 2024). Supply of methane to surface waters through lateral transport from shallower areas is also not expected in this coastal system. The rate of accumulation of fine-grained, organic-rich sediment and, hence of anaerobic degradation of organic matter, decreases with decreasing water depth in the lake (Sulu-Gambari et al., 2017). This implies that, at shallow sites, there is less methanogenesis in the sediment and less potential for its escape to the overlying water than at deep sites.

In June, the distinct counter gradients in oxygen and methane and strong shift in $\delta^{13}C$ – CH_4 and δD–CH_4 towards higher values at the oxycline (Fig. 2) point towards aerobic removal. Aerobic methanotrophy is common in many stratified systems (Mau et al., 2013; Reis et al., 2020) and was observed at the oxycline in the water column of Scharendijke basin previously (Żygadłowska et al., 2023; Venetz et al., 2023). In July and August, however, the oxycline was located at a shallower depth, and an increase in $\delta^{13}C$ – CH_4 and δD – CH_4 values was observed in the suboxic zone below the oxycline, suggesting methane removal in the absence of oxygen. However, as noted above, we speculate that there still could have been some oxygen supply to this zone through both vertical and lateral transport, implying that some of the methane removal could still have been aerobic. Nitrate and nitrite were unlikely to be acting as electron acceptors in methane oxidation in the suboxic zone since concentrations of both solutes were low (<1.1 μmol L^{-1}) and the relative abundance of nitrifiers was low as well (Venetz et al., 2024). This implies little turnover of nitrate and nitrite in the water column. Notably, the enrichment of particulate iron near the oxycline and increase of dissolved iron below the oxycline (Fig. 2) point towards active iron cycling, as is common in anoxic, sulfide-free zones in anoxic basins (Millero, 1991). There was no evidence for iron reducing bacteria other than MOB of the *Methylomonadaceae* family, which were observed in high numbers below the oxycline (Fig. 2). These seemingly aerobic microbes have also been found to be capable of methane oxidation coupled to iron oxide reduction in oxygen-deprived conditions (Li et al., 2023). Only few methanotrophic archaea were present (Table S1). Hence, we conclude that in July and August, the *Methylomonadaceae* may have been involved in both aerobic and anaerobic removal of methane, with the latter process possibly linked to iron reduction. Again, methane was present in the surface waters (0.06–0.25 μmol L^{-1}), which indicates incomplete removal of methane.

At the end of August and in September, the stratification weakened further and the water column slowly began to mix. The physical mixing of the water column enhanced upward transport of methane resulting in high surface water methane concentrations (0.25 and 0.4 μmol L^{-1}). *Methylomonadaceae* were still abundant below the oxycline, indicating there could have been methane removal below the oxycline as well. This was likely aerobic, since there is no evidence for iron cycling at this time (Fig. 2). High concentrations of nitrate and nitrite (Fig. 2) were observed in the suboxic zone at the end of August, which could have resulted from a sudden nitrification event. Indeed *Nitrosomonodaceae*, which are capable of ammonium oxidation to nitrite, emerged in the waters

around the oxycline at the end of August (Venetz et al., 2024). Notably, there was no sign of *Methylomirabilis oxyfera* – the methanotrophs that can couple methane oxidation to nitrite reduction (Ettwig et al., 2010), nor was there a change in the abundance of *Methanoperedenaceae* (Table S1; Venetz et al., 2024). This suggests that the *Methylomonadaceae* still accounted for the methane removal near the oxycline.

The isotopic fractionation factors calculated for the zone where enrichments in ^{13}C were observed in the summer ranged from 1.006 to 1.014 (Section S2.4; Table S3). These values are within the lower range of fractionation factors reported for aerobic and anaerobic methane oxidation (1.002–1.035; Grant and Whiticar, 2002). The fractionation factors are likely strongly affected by bubble dissolution since dissolving bubbles are expected to shift the isotopic signature towards lower values (Leonte et al., 2018). While the crossplot of $\delta^{13}C - CH_4$ and $\delta D - CH_4$ points towards methane oxidation, a positive isotopic shift in $\delta^{13}C - CH_4$ and $\delta D - CH_4$ values is only observed at low methane concentrations in the waters above the oxycline (Figs. 2 and 5A). Methane removal in other parts of the water column is not associated with a positive isotopic shift, in line with a control of methane transport in the water column by physical processes such as ebullitive transport.

Methane concentrations observed in the surface waters were relatively high (Figure S5) when compared to other coastal systems (e.g. Steinsdóttir et al., 2022), which likely is due to bubble dissolution. In summer, we observe $\delta^{13}C - CH_4$ and $\delta D\text{-}CH_4$ values above the oxycline similar to those in the bottom water with bubble dissolution accounting for up to 94 % of the methane (Table 2). Although the concentrations found in the surface waters are generally low, when compared to the rest of the water column, this suggests that bubble dissolution plays a critical role in methane supply to the surface waters and, subsequently, the release of methane to the atmosphere. Apparently, MOB were unable to establish in the surface waters between March and October and hence were not able to efficiently remove the methane despite unlimited oxygen availability.

4.3. Methane fluxes to the atmosphere

The measured in-situ diffusive fluxes of methane to the atmosphere and the calculated diffusive fluxes of methane to the atmosphere were not only of the same order of magnitude, but also showed the same seasonal trend (Fig. 4). All the fluxes were relatively high (0.01 – 1.15 mmol m^{-2} d^{-1}) when compared to the average flux of methane to the atmosphere for continental shelves (0.03 mmol m^{-2} d^{-1}; Bange et al., 1994), but comparable to other coastal systems (e.g. 0.02 – 0.64 mmol m^{-2} d^{-1} in By Fjord, Bonaglia et al., 2022; 0.07 – 0.39 mmol m^{-2} d^{-1} in Pojo Bay, Myllykangas et al., 2020; 0.01 – 0.75 mmol m^{-2} d^{-1} in the Boknis Eck, Ma et al., 2020).

We find the highest fluxes in spring, when the water column was still well-mixed, and upon the onset of mixing of the stratified water column from end of August onwards (Figs. 4 and 6). The high release in spring is in line with previous work showing that upward transport of dissolved methane can be very efficient in well-mixed water columns and can support high fluxes of methane to the atmosphere (Borges et al., 2016). Enhanced release of methane to the atmosphere after a period of stratification was previously observed in Chesapeake Bay (Gelesh et al., 2016) where very similar surface water concentrations (0.4 μmol L^{-1}) and diffusive fluxes (1.8 mmol m^{-2} d^{-1}) were observed.

At Scharendijke basin, the vast majority of the methane is released from the sediments in the form of bubbles, however (Table 3). The efficiency of the microbial filter in the water column, defined as the percentage of methane that is released from the sediment but does not escape to the atmosphere, is therefore highly dependent on the extent of dissolution of the methane bubbles. Methane emissions at our site through bubble release are approximately 30–100 times higher than methane emissions via diffusion only (Table 3), thereby reducing the efficiency of the microbial methane filter. High bubble fluxes and a large bubble diameter are known to correlate (Delwiche and Hemond, 2017). Large bubbles not only carry more methane within their volume but are also much more resistant to dissolution and rise faster through the water column than smaller bubbles. This increases their chances of reaching the atmosphere without losing much methane on the way (DelSontro et al., 2015).

Our model calculations suggest a potential year-round ebullitive flux of 30–120 mmol m^{-2} d^{-1} (Table 3). The bubble flux based on bubbles caught in the floating chamber during the measurements varied more widely from 0.5 to 245 mmol m^{-2} d^{-1} (Table 4). Both methods give an order of magnitude range for the bubble flux only. The model fluxes rely on an assumption of the diameter of the bubbles, which is largely unknown. Not all ebullition events in the floating chamber were monitored for their methane release, hence the number of observations from which we extrapolate the flux is relatively limited. Nevertheless, the largely overlapping ranges of the methane bubble fluxes support our conclusion that ebullition is a major contributor to methane emissions at this site.

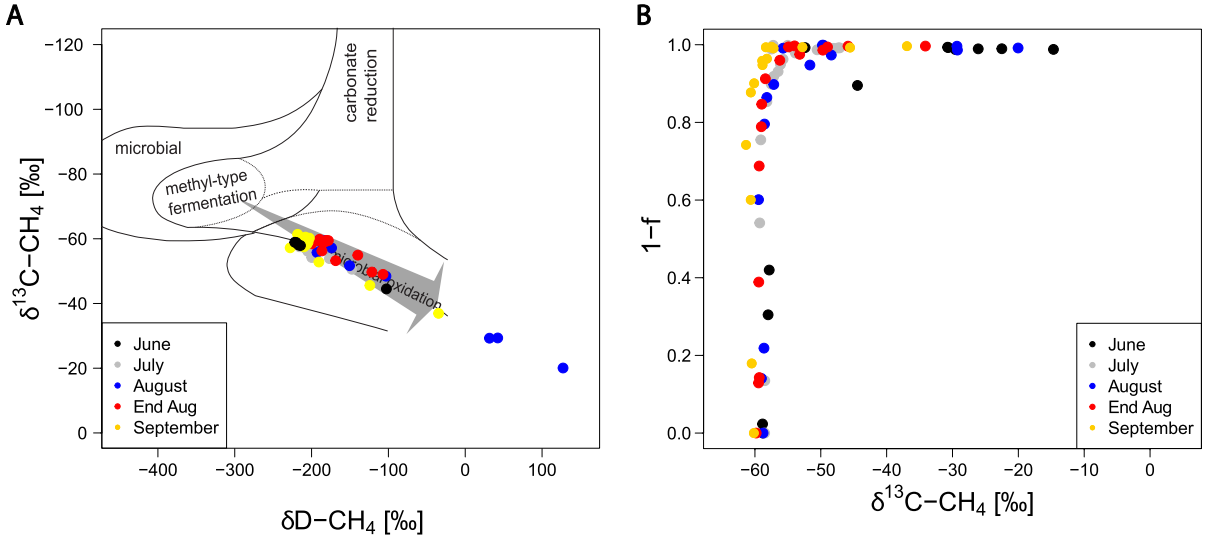

Fig. 5. A) Isotopic composition of methane ($\delta^{13}C\text{-}CH_4$ and $\delta D\text{-}CH_4$), with the background modified from Whiticar (1999) and Egger et al. (2017). The grey arrow indicates the direction of the shift in isotopic composition due to microbial methane oxidation (Whiticar, 1999). B) The fraction of methane removed (1-f) as a function of $\delta^{13}C$ of methane where f stands for the concentration of methane in a sample relative to the bottom water methane, illustrating the strong effect of bubble dissolution on the isotopic signature.

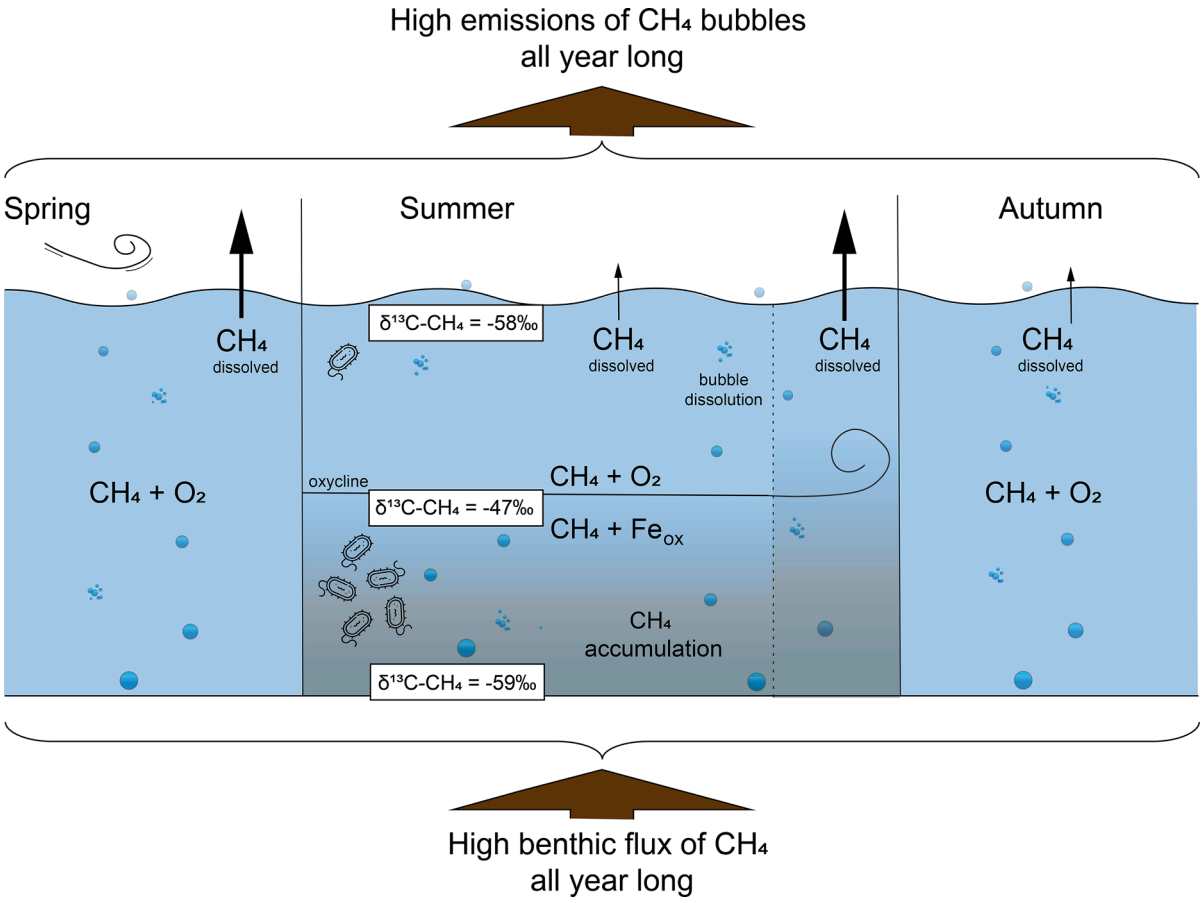

Fig. 6. Schematic of methane dynamics at Scharendijke basin. In spring the release of dissolved methane to the atmosphere is enhanced by wind-mixing. Summer stratification acts as a barrier and traps methane in the bottom waters, decreasing its diffusive release to the atmosphere. The low δ^{13}C-CH_4 values in the surface waters (here for July) reflect bubble dissolution. The breaking of stratification at the end of summer leads to release of the accumulated methane and results in high diffusive fluxes of methane to the atmosphere. Methane bubble emissions are high all year round regardless of the water column dynamics.

Bubble fluxes of a similar order of magnitude have been reported for the highly eutrophic Dalian Bay (74 mmol m^{-2} d^{-1}; Kunpeng et al., 2019), and eutrophic Lake Wohlen (45 mmol m^{-2} d^{-1}; DelSontro et al., 2015).

5. Conclusions

Based on our methane flux measurements and model results we conclude that a large proportion of the methane released from the sediment in Scharendijke basin bypasses the microbial filter in the water column in the form of bubbles and is released directly to the atmosphere. The ebullitive flux of methane to the atmosphere exceeds the diffusive flux and may range up to 120 mmol m^{-2} d^{-1}. Shifts in δ^{13}C–CH_4 and δD-CH_4 to higher values near the oxycline during summer stratification and the abundant presence of methane oxidizing bacteria point towards microbial removal of methane. In June, most removal of dissolved methane occurs aerobically. In July and August, an additional role for anaerobic methanotrophy, possibly linked to iron oxide reduction, is suggested. We find no evidence for a role of nitrate or nitrite as an electron acceptor nor for a major role of archaea in removal of methane in the water column of this coastal system. The depletion in δ^{13}C – CH_4 and δD – CH_4 observed in the waters above the oxycline suggests that bubble dissolution contributes to elevated methane concentrations in the surface waters. As deoxygenation and eutrophication in the coastal ocean continue to advance (Breitburg et al., 2018), a growing number of coastal environments may witness a shift towards conditions in which ebullition accounts for the major proportion of the benthic methane flux and methane emissions to the atmosphere. As a consequence, the role of coastal systems as a source of methane to the atmosphere is expected to increase in future.

6. Data availability

Data are available through Zenodo at https://zenodo.org/doi/10.5281/zenodo.10034518. Sequence data has been submitted to the European Nucleotide Archive under accession number PRJEB67906 (https://www.ebi.ac.uk/ena/browser/view/PRJEB67906).

CRediT authorship contribution statement

Olga M. Żygadłowska: Writing – review & editing, Writing – original draft, Visualization, Methodology, Investigation, Formal analysis, Data curation. **Jessica Venetz:** Writing – review & editing, Methodology, Investigation, Formal analysis, Data curation. **Wytze K. Lenstra:** Writing – review & editing, Methodology, Investigation, Formal analysis, Data curation. **Niels A.G.M. van Helmond:** Writing – review & editing, Methodology, Investigation, Data curation. **Robin Klomp:** Writing – review & editing, Methodology, Investigation, Data curation. **Thomas Röckmann:** Writing – review & editing, Methodology, Investigation. **Annelies J. Veraart:** Writing – review & editing, Methodology, Investigation, Conceptualization. **Mike S.M. Jetten:** Writing – review & editing, Supervision, Project administration, Investigation, Funding acquisition, Data curation, Conceptualization. **Caroline P. Slomp:** Writing – review & editing, Writing – original draft, Supervision, Project administration, Methodology, Investigation, Funding acquisition, Formal analysis, Data curation, Conceptualization.

Declaration of competing interest

The authors declare that they have no known competing financial interests or personal relationships that could have appeared to influence the work reported in this paper.

Acknowledgements

We thank the captain and crew of the R/V Navicula, Y. Witte and other staff of the Royal Netherlands Institute for Sea Research (NIOZ) for their support during the sampling campaigns. We are also grateful to J. Visser, H. de Waard, T. Claessen, C. van der Veen, E. Heiskanen, R. Puyk and Y. Chung for analytical assistance in Utrecht. This research was financially supported by European Research Council Synergy grant MARIX (854088) and H2020 Marie Skłodowska-Curie COFUND program (847504). This work was carried out under the program of the Netherlands Earth System Science Center (NESSC 024002001) and SIAM (024002002), financially supported by the Ministry of Education, Culture and Science (OCW). WKL acknowledges funding by the Dutch Research Council (NWO VI.Veni.212.040). The authors declare that the research was conducted in the absence of any commercial or financial relationships that could be construed as a potential conflict of interest.

Appendix A. Supplementary material

Supplementary material to this article can be found online at https://doi.org/10.1016/j.gca.2024.08.028.

References

Bange, H.W., Bartell, U.H., Rapsomanikis, S., Andreae, M.O., 1994. Methane in the Baltic and North Seas and a reassessment of the marine emissions of methane. North 8, 465–480.

Bastviken, D., Cole, J., Pace, M., Tranvik, L., 2004. Methane emissions from lakes: dependence of lake characteristics, two regional assessments, and a global estimate. Global Biogeochem. Cycles 18, 1–12.

Beal, E.J., House, C.H., Orphan, V.J., 2009. Manganese-and iron-dependent marine methane oxidation. Science 325, 184–187.

Boetius, A., Ravenschlag, K., Schubert, C.J., Rickert, D., Widdel, F., Gleeske, A., Amann, R., Jorgensen, B.B., Witte, U., Pfannkuche, O., 2000. A marine microbial consortium apparently mediating AOM. Nature 407, 623–626.

Bonaglia, S., Rütting, T., Kononets, M., Stigebrandt, A., Santos, I.R., Hall, P.O.J., 2022. High methane emissions from an anoxic fjord driven by mixing and oxygenation. Limnol. Oceanogr. Lett. 7, 392–400.

Borges, A.V., Champenois, W., Gypens, N., Delille, B., Harlay, J., 2016. Massive marine methane emissions from near-shore shallow coastal areas. Sci. Rep. 6, 2–9.

Boudreau, B.P., 1996. The diffusive tortuosity of fine-grained unlithified sediments. Geochim. Cosmochim. 60, 3139–3142.

Boudreau, B.P., Algar, C., Johnson, B.D., Croudace, I., Reed, A., Furukawa, Y., Dorgan, K. M., Jumars, P.A., Grader, A.S., Gardiner, B.S., 2005. Bubble growth and rise in soft sediments. Geology 33, 517–520.

Brass, M., Röckmann, T., 2010. Continuous-flow isotope ratio mass spectrometry method for carbon and hydrogen isotope measurements on atmospheric methane. Atmos. Meas. Tech. 3, 1707–1721.

Breitburg, D., Levin, L.A., Oschlies, A., Grégoire, M., Chavez, F.P., Conley, D.J., Garçon, V., Gilbert, D., Gutiérrez, D., Isensee, K., Jacinto, G.S., Limburg, K.E., Montes, I., Naqvi, S.W.A., Pitcher, G.C., Rabalais, N.N., Roman, M.R., Rose, K.A., Seibel, B.A., Telszewski, M., Yasuhara, M., Zhang, J., 2018. Declining oxygen in the global ocean and coastal waters. Science 359, eaam7240.

Burdige, D.J., 2006. Geochemistry of Marine Sediments. Princeton University Press.

Cline, J.D., 1969. Spectrophotometric determination of hydrogen sulfide in natural waters 1. Limnol. Oceanogr. 14, 454–458.

Coleman, D.D., Risatti, J.B., Schoell, M., 1981. Fractionation of carbon and hydrogen isotopes by methane-oxidizing bacteria. Geochim. Cosmochim. Acta 45, 1033–1037.

Crill, P.M., Martens, C.S., 1987. Biogeochemical cycling in an organic-rich coastal marine basin. 6. Temporal and spatial variations in sulfate reduction rates. Geochim. Cosmochim. Acta 51, 1175–1186.

Cutter, G.A., Casciotti, K., Croot, P., Geibert, W., Heimbürger, L.-E., Lohan, M.C., Planquette, H., van de Flierdt, T., 2017. Sampling and sample-handling protocols for GEOTRACES Cruises, Version 3.0.

D'Ambrosio, S.L., Harrison, J.A., 2022. Measuring CH4 fluxes from lake and reservoir sediments: methodologies and needs. Front. Environ. Sci. 10, 1–19.

Dale, A.W., Cappellen, P., Van, A.D.R., Regnier, P., 2008. Methane efflux from marine sediments in passive and active margins: estimations from bioenergetic reaction – transport simulations. Earth Planet. Sci. Lett. 265, 329–344.

Delsontro, T., McGinnis, D.F., Wehrli, B., Ostrovsky, I., 2015. Size does matter: importance of large bubbles and small-scale hot spots for methane transport. Environ. Sci. Technol. 49, 1268–1276.

Delwiche, K.B., Hemond, H.F., 2017. Methane bubble size distributions, flux, and dissolution in a freshwater lake. Environ. Sci. Technol. 51, 13733–13739.

Egger, M., Lenstra, W., Jong, D., Meysman, F.J.R., Sapart, C.J., Van Der Veen, C., Röckmann, T., Gonzalez, S., Slomp, C.P., 2016. Rapid sediment accumulation results in high methane effluxes from coastal sediments. PLoS One 11, 1–22.

Egger, M., Hagens, M., Sapart, C.J., Dijkstra, N., van Helmond, N.A.G.M., Mogollón, J.M., Risgaard-Petersen, N., van der Veen, C., Kasten, S., Riedinger, N., Böttcher, M.E., Röckmann, T., Jørgensen, B.B., Slomp, C.P., 2017. Iron oxide reduction in methane-rich deep Baltic Sea sediments. Geochim. Cosmochim. Acta 207, 256–276.

Ettwig, K.F., Van Alen, T., van de Pas-Schoonen, K.T., Jetten, M.S.M., Strous, M., 2009. Enrichment and molecular detection of denitrifying methanotrophic bacteria of the NC10 phylum. Appl. Environ. Microbiol. 75, 3656–3662.

Ettwig, K.F., Butler, M.K., Le Paslier, D., Pelletier, E., Mangenot, S., Kuypers, M.M.M., Schreiber, F., Dutilh, B.E., Zedelius, J., De Beer, D., Gloerich, J., Wessels, H.J.C.T., Van Alen, T., Luesken, F., Wu, M.L., Van De Pas-Schoonen, K.T., Op Den Camp, H.J. M., Janssen-Megens, E.M., Francoijs, K.J., Stunnenberg, H., Weissenbach, J., Jetten, M.S.M., Strous, M., 2010. Nitrite-driven anaerobic methane oxidation by oxygenic bacteria. Nature 464, 543–548.

Ettwig, K.F., Zhu, B., Speth, D., Keltjens, J.T., Jetten, M.S.M., Kartal, B., 2016. Archaea catalyze iron-dependent anaerobic oxidation of methane. Proc. Natl. Acad. Sci. u. s. a. 113, 12792–12796.

Froelich, P.N., Klinkhammer, G.P., Bender, M.L., Luedtke, N.A., Heath, G.R., Cullen, D., Dauphin, P., Hammond, D., Hartman, B., Maynard, V., 1979. Early oxidation of organic matter in pelagic sediments of the eastern equatorial Atlantic: suboxic diagenesis. Geochim. Cosmochim. Acta 43, 1075–1090.

Gelesh, L., Marshall, K., Boicourt, W., Lapham, L., 2016. Methane concentrations increase in bottom waters during summertime anoxia in the highly eutrophic estuary, Chesapeake Bay, U.S.A. Limnol. Oceanogr. 61, S253–S266.

Grant, N.J., Whiticar, M.J., 2002. Stable carbon isotopic evidence for methane oxidation in plumes above Hydrate Ridge, Cascadia Oregon Margin. Global Biogeochem. Cycles 16, 71-1-71–13.

Grégoire, M., Garçon, V., Garcia, H., Breitburg, D., Isensee, K., Oschlies, A., Telszewski, M., Barth, A., Bittig, H.C., Carstensen, J., Carval, T., Chai, F., Chavez, F., Conley, D., Coppola, L., Crowe, S., Currie, K., Dai, M., Deflandre, B., Dewitte, B., Diaz, R., Garcia-Robledo, E., Gilbert, D., Giorgetti, A., Glud, R., Gutierrez, D., Hosoda, S., Ishii, M., Jacinto, G., Langdon, C., Lauvset, S.K., Levin, L.A., Limburg, K. E., Mehrtens, H., Montes, I., Naqvi, W., Paulmier, A., Pfeil, B., Pitcher, G., Pouliquen, S., Rabalais, N., Rabouille, C., Recape, V., Roman, M., Rose, K., Rudnick, D., Rummer, J., Schmechtig, C., Schmidtko, S., Seibel, B., Slomp, C., Sumalia, U.R., Tanhua, T., Thierry, V., Uchida, H., Wanninkhof, R., Yasuhara, M., 2021. A global ocean oxygen database and atlas for assessing and predicting deoxygenation and ocean health in the open and Coastal Ocean. Front. Mar. Sci. 8.

Hagens, M., Slomp, C.P., Meysman, F.J.R., Seitaj, D., Harlay, J., Borges, A.V., Middelburg, J.J., 2015. Biogeochemical processes and buffering capacity concurrently affect acidification in a seasonally hypoxic coastal marine basin. Biogeosciences 12, 1561–1583.

Haroon, M.F., Hu, S., Shi, Y., Imelfort, M., Keller, J., Hugenholtz, P., Yuan, Z., Tyson, G. W., 2013. Anaerobic oxidation of methane coupled to nitrate reduction in a novel archaeal lineage. Nature 500, 567–570.

Humborg, C., Geibel, M.C., Sun, X., McCrackin, M., Mörth, C.M., Stranne, C., Jakobsson, M., Gustafsson, B., Sokolov, A., Norkko, A., Norkko, J., 2019. High emissions of carbon dioxide and methane from the coastal Baltic Sea at the end of a summer heat wave. Front. Mar. Sci. 6, 1–14.

Imboden, D.M., Wüest, A., 1995. Mixing Mechanisms in Lakes. Phys. Chem. Lakes 83–138.

Jørgensen, B.B., Beulig, F., Egger, M., Petro, C., Scholze, C., Røy, H., 2019. Organoclastic sulfate reduction in the sulfate-methane transition of marine sediments. Geochim. Cosmochim. Acta 254, 231–245.

Jorgensen, B.B., 1980. Seasonal Oxygen Depletion in the Bottom Waters of a Danish Fjord and Its Effect on the Benthic Community Author (s): Bo Barker Jørgensen Published by : Wiley on behalf of Nordic Society. Oikos 34, 68–76.

Joye, S.B., Boetius, A., Orcutt, B.N., Montoya, J.P., Schulz, H.N., Erickson, M.J., Lugo, S. K., 2004. The anaerobic oxidation of methane and sulfate reduction in sediments from Gulf of Mexico cold seeps. Chem. Geol. 205, 219–238.

Judd, A., Davies, G., Wilson, J., Holmes, R., Baron, G., Bryden, I., 1997. Erratum : Contributions to atmospheric methane by natural seepages on the U.K continental shelf. Mar. Geol. 140, 427–455.

Kanwischer, M., Klintzsch, T., Schmale, O., 2023. Stable isotope approach to assess the production and consumption of methylphosphonate and its contribution to oxic methane formation in surface waters. Environ. Sci. Technol. 57, 15904–15913.

Kemp, W.M., Sampou, P.A., Garber, J., Tuttle, J., Boynton, W.R., 1992. Seasonal depletion of oxygen from bottom waters of Chesapeake Bay: roles of benthic and planktonic respiration and physical exchange processes. Mar. Ecol. Prog. Ser. 85, 137–152.

Kiene, R.P., Capone, D.G., 1985. Degassing of pore water methane during sediment incubations. Appl. Environ. Microbiol. 49, 143–147.

Klump, J.V., Martens, C.S., 1980. Biogeochemical cycling in an organic-rich coastal marine basin—I. Methane sediment-water exchange processes. Geochim. Cosmochim. Acta 44 (3), 471–490.

Knittel, K., Boetius, A., 2009. Anaerobic oxidation of methane: progress with an unknown process. Annu. Rev. Microbiol. 63, 311–334.

Kunpeng, Z., Nan, Z., Xuemei, X., Lingxi, Z., Juying, W., 2019. Bubble-mediated methane release from polluted Dalian Bay in China in summer, 2016. Cont. Shelf Res. 185, 51–56.

Lan, X., Thoning, K.W., Dlugokencky, E.J., 2024. Trends in globally-averaged CH_4, N_2O, and SF6 determined from NOAA Global Monitoring Laboratory measurements. *Glob. Monit. Lab.* **6**.

Leifer, I., Patro, R.K., 2002. The bubble mechanism for methane transport from the shallow sea bed to the surface: A review and sensitivity study. Cont. Shelf Res. 22, 2409–2428.

Lenstra, W.K., Hermans, M., Séguret, M.J.M., Witbaard, R., Severmann, S., Behrends, T., Slomp, C.P., 2021. Coastal hypoxia and eutrophication as key controls on benthic release and water column dynamics of iron and manganese. Limnol. Oceanogr. 66, 807–826.

Lenstra, W.K., van Helmond, N.A.G.M., Żygadłowska, O.M., van Zummeren, R., Witbaard, R., Slomp, C.P., 2022. Sediments as a Source of Iron, Manganese, Cobalt and Nickel to Continental Shelf Waters (Louisiana, Gulf of Mexico). Front. Mar. Sci. 9, 1–32.

Lenstra, W.K., Van Helmond, N.A.G.M., Dalcin, M.P., Wallenius, A.J., Jetten, M.S.M., Slomp, C.P., 2023. Gene-based modeling of methane oxidation in coastal sediments: constraints on the efficiency of the microbial methane filter. Environ. Sci. Technol. 57, 12722–12731.

Leonte, M., Wang, B., Socolofsky, S.A., Mau, S., Breier, J.A., Kessler, J.D., 2018. Using carbon isotope fractionation to constrain the extent of methane dissolution into the water column surrounding a natural hydrocarbon gas seep in the Northern Gulf of Mexico. Geochem. Geophys. Geosyst. 19, 4459–4475.

Leu, A.O., Cai, C., Mcilroy, S.J., Hu, S., Tyson, G.W., Tyson, G.W., 2020. Anaerobic methane oxidation coupled to manganese reduction by members of the Methanoperedenaceae. ISME J. 14, 1030–1041.

Li, B., Tao, Y., Mao, Z., Gu, Q., Han, Y., Hu, B., Wang, H., Lai, A., Xing, P., Wu, Q.L., 2023. Iron oxides act as an alternative electron acceptor for aerobic methanotrophs in anoxic lake sediments. Water Res. 234, 119833.

Ma, X., Sun, M., Lennartz, S.T., Bange, H.W., 2020. A decade of methane measurements at the Boknis Eck time series station in Eckernförde Bay (southwestern Baltic Sea). Biogeosciences 17, 3427–3438.

Mau, S., Blees, J., Helmke, E., Niemann, H., Damm, E., 2013. Vertical distribution of methane oxidation and methanotrophic response to elevated methane concentrations in stratified waters of the Arctic fjord Storfjorden (Svalbard, Norway). Biogeosciences 10, 6267–6268.

McGinnis, D.F., Greinert, J., Artemov, Y., Beaubien, S.E., Wüest, A., 2006. Fate of rising methane bubbles in stratified waters: How much methane reaches the atmosphere? J. Geophys. Res. Ocean. 111, C09007.

Millero, F.J., 1991. The oxidation of H_2S with O_2 in the Black Sea. Black Sea Oceanogr. 205–227.

Myllykangas, J.P., Hietanen, S., Jilbert, T., 2020. Legacy effects of eutrophication on modern methane dynamics in a boreal estuary. Estuar. Coasts 43, 189–206.

Naqvi, S.W.A., Bange, H.W., Farias, L., Monteiro, P.M.S., Scranton, M.I., Zhang, J., 2010. Marine hypoxia/anoxia as a source of CH_4 and N_2O. Biogeosciences 7, 2159–2190.

Ostrovsky, I., Mcginnis, D.F., Lapidus, L., Eckert, W., 2008. Quantifying gas ebullition with echosounder: The role of methane transport by bubbles in a medium-sized lake. Limnol. Oceanogr. Methods 6, 105–118.

Padilla, C.C., Bristow, L.A., Sarode, N., Garcia-Robledo, E., Gómez, R.E., Benson, C.R., Bourbonnais, A., Altabet, M.A., Girguis, P.R., Thamdrup, B., Stewart, F.J., 2016. NC10 bacteria in marine oxygen minimum zones. ISME J. 10, 2067–2071.

Padilla, C.C., Bertagnolli, A.D., Bristow, L.A., Sarode, N., Glass, J.B., Thamdrup, B., Stewart, F.J., 2017. Metagenomic binning recovers a transcriptionally active gammaproteobacterium linking methanotrophy to partial denitrification in an anoxic oxygen minimum zone. Front. Mar. Sci. 4, 1–15.

Perez-Coronel, E., Benan, M.J., 2022. Multiple sources of aerobic methane production in aquatic ecosystems include bacterial photosynthesis. Nat. Commun. 13, 6454.

Read, J.S., Hamilton, D.P., Desai, A.R., Rose, K.C., MacIntyre, S., Lenters, J.D., Smyth, R. L., Hanson, P.C., Cole, J.J., Staehr, P.A., Rusak, J.A., Pierson, D.C., Brookes, J.D., Laas, A., Wu, C.H., 2012. Lake-size dependency of wind shear and convection as controls on gas exchange. Geophys. Res. Lett. 39, 1–5.

Reeburgh, W., 1969. Observation of gases in Chesapeake Bay sediments. Limnol. Oceanogr. 14, 317–474.

Reeburgh, W.S., 2007. Oceanic methane biogeochemistry. Chem. Rev. 107, 486–513.

Reeburgh, W.S., Ward, B.B., Whalen, S.C., Sandbeck, K.A., Kilpatrickt, K.A., Kerkhof, L. J., 1991. Black Sea methane geochemistry. Deep Sea Res. Part A. Oceanogr. Res. Pap. 38, S1189–S1210.

Reindl, A.R., Bolałek, J., 2014. Methane flux from sediment into near-bottom water and its variability along the Hel Peninsula-Southern Baltic Sea. Cont. Shelf Res. 74, 88–93.

Reis, P.C.J., Ruiz-González, C., Crevecoeur, S., Soued, C., Prairie, Y.T., 2020. Rapid shifts in methanotrophic bacterial communities mitigate methane emissions from a tropical hydropower reservoir and its downstream river. Sci. Total Environ. 748, 141374.

Resplandy, L., Hogikyan, A., Müller, J.D., Najjar, R.G., Bange, H.W., Bianchi, D., Weber, T., Cai, W.J., Doney, S.C., Fennel, K., Gehlen, M., Hauck, J., Lacroix, F., Landschützer, P., Le Quéré, C., Roobaert, A., Schwinger, J., Berthet, S., Bopp, L., Chau, T.T.T., Dai, M., Gruber, N., Ilyina, T., Kock, A., Manizza, M., Lachkar, Z., Laruelle, G.G., Liao, E., Lima, I.D., Nissen, C., Rödenbeck, C., Séférian, R., Toyama, K., Tsujino, H., Regnier, P., 2024. A Synthesis of Global Coastal Ocean Greenhouse Gas Fluxes. Global Biogeochem. Cycles 38, 1–38.

Rosentreter, J.A., Borges, A.V., Deemer, B.R., Holgerson, M.A., Liu, S., Song, C., Melack, J., Raymond, P.A., Duarte, C.M., Allen, G.H., Olefeldt, D., Poulter, B., Battin, T.I., Eyre, B.D., 2021. Half of global methane emissions come from highly variable aquatic ecosystem sources. Nat. Geosci. 14, 225–230.

Sapart, C.J., Van Der Veen, C., Vigano, I., Brass, M., Van De Wal, R.S.W., Bock, M., Fischer, H., Sowers, T., Buizert, C., Sperlich, P., Blunier, T., Behrens, M., Schmitt, J., Seth, B., Röckmann, T., 2011. Simultaneous stable isotope analysis of methane and nitrous oxide on ice core samples. Atmos. Meas. Tech. 4, 2607–2618.

Saunois, M., Stavert, A.R., Poulter, B., Bousquet, P., Canadell, J.G., Jackson, R.B., Raymond, P.A., Dlugokencky, E.J., Houweling, S., Patra, P.K., et al., 2020. The global methane budget 2000–2017. Earth Syst. Sci. Data 12, 1561–1623.

Schmale, O., Schneider Von Deimling, J., Gülzow, W., Nausch, G., Waniek, J.J., Rehder, G., 2010. Distribution of methane in the water column of the Baltic Sea. Geophys. Res. Lett. 37, 1–5.

Sivan, O., Adler, M., Pearson, A., Gelman, F., Bar-Or, I., John, S.G., Eckert, W., 2011. Geochemical evidence for iron-mediated anaerobic oxidation of methane. Limnol. Oceanogr. 56, 1536–1544.

Soetaert, K., Petzoldt, T., Setzer, R.W., 2010. Solving differential equations in R: package deSolve. J. Stat. Softw. 33, 1–25.

Solorzano, L., 1969. Determination of ammonia in natural waters by the phenolhypochlorite method. This research was fully supported by US Atomic Energy Commission Contract No. ATS (11–1) GEN 10, PA 20. Limnol. Oceanogr. 14, 799–801.

Steinle, L., Maltby, J., Treude, T., Kock, A., Bange, H.W., Engbersen, N., Zopfi, J., Lehmann, M.F., Niemann, H., 2017. Effects of low oxygen concentrations on aerobic methane oxidation in seasonally hypoxic coastal waters. Biogeosciences 14, 1631–1645.

Steinsdóttir, H.G.R., Schauberger, C., Mhatre, S., Thamdrup, B., Bristow, L.A., 2022. Aerobic and anaerobic methane oxidation in a seasonally anoxic basin. Limnol. Oceanogr. 67, 1257–1273.

Sulu-Gambari, F., Roepert, A., Jilbert, T., Hagens, M., Meysman, F.J.R., Slomp, C.P., 2017. Molybdenum dynamics in sediments of a seasonally-hypoxic coastal marine basin. Chem. Geol. 466, 627–640.

Thamdrup, B., Steinsdóttir, H.G.R., Bertagnolli, A.D., Padilla, C.C., Patin, N.V., Garcia-Robledo, E., Bristow, L.A., Stewart, F.J., 2019. Anaerobic methane oxidation is an important sink for methane in the ocean's largest oxygen minimum zone. Limnol. Oceanogr. 64, 2569–2585.

Turner, R.E., Schroeder, W.W., Wiseman, W.J., 1987. The role of stratification in the deoxygenation of Mobile Bay and adjacent shelf bottom waters. Estuaries 10, 13–19.

Venetz, J., Żygadłowska, O.M., Lenstra, W.K., van Helmond, N.A.G.M., Nuijten, G.H.L., Wallenius, A.J., Dalcin, M.P., Slomp, C.P., Jetten, M.S.M., Veraart, A.J., 2023. Versatile methanotrophs form an active methane biofilter in the oxycline of a seasonally stratified coastal basin. Environ. Microbiol. 25, 2277–2288.

Venetz, J., Żygadłowska, O.M., Dotsios, N., Wallenius, A.J., van Helmond, N.A.G.M., Lenstra, W.K., Klomp, R., Slomp, C.P., Jetten, M.S.M., Veraart, A.J., 2024. Seasonal dynamics of the microbial methane filter in the water column of a eutrophic coastal basin. FEMS Microbiol. Ecol. 100, fiae007.

Wallace, P.J., Dickens, G.R., Paull, C.K., Ussler, W., 2000. Effects of core retrieval and degassing on the carbon isotope composition of methane in gas hydrate-and free gas-bearing sediments from the Blake Ridge. Proc. Ocean Drill. Program. Sci. Results 164, 101–112.

Wallenius, A.J., Dalcin, M.P., Slomp, C.P., Jetten, M.S.M., 2021. Anthropogenic and Environmental Constraints on the Microbial Methane Cycle in Coastal Sediments. Front. Microbiol. 12, 631621.

Weber, T., Wiseman, N.A., Kock, A., 2019. Global ocean methane emissions dominated by shallow coastal waters. Nat. Commun. 10, 1–10.

Whiticar, M.J., 1999. Carbon and hydrogen isotope systematics of bacterial formation and oxidation of methane. Chem. Geol. 161, 291–314.

Whiticar, M.J., Faber, E., 1986. Methane oxidation in sediment and water column environments-Isotope evidence. Org. Geochem. 10, 759–768.

Wik, M., Crill, P.M., Varner, R.K., Bastviken, D., 2013. Multiyear measurements of ebullitive methane flux from three subarctic lakes. J. Geophys. Res. Biogeosciences 118, 1307–1321.

Żygadłowska, O.M., Venetz, J., Klomp, R., Lenstra, W.K., van Helmond, N.A.G.M., Röckmann, T., Wallenius, A.J., Martins, P.D., Veraart, A.J., Jetten, M.S.M., Slomp, C. P., 2023. Pathways of methane removal in the sediment and water column of a seasonally anoxic eutrophic marine basin. Front. Mar. Sci. 10, 1–15.